Turkish Journal of Engineering & Environmental Sciences

http://journals.tubitak.gov.tr/engineering/

Research Article

Turkish J Eng Env Sci
(2014) 38: 411 – 433

doi:10.3906/muh-1407-24

Effects of higher order Taylor series terms on the solution accuracy of NI-RPIM for 3D elastostatic problems

Mustafa Murat YAVUZ[1], **Bahattin KANBER**[2,*]

[1]Department of Energy Systems Engineering, Faculty of Engineering, Osmaniye Korkut Ata University, Osmaniye, Turkey

[2]Department of Mechanical Engineering, Faculty of Engineering, Gaziantep University, Gaziantep, Turkey

Received: 21.07.2014 • **Accepted/Published Online:** 09.12.2015 • **Printed:** 04.03.2016

Abstract: Effects of higher order Taylor series terms of the nodal integration-radial point interpolation method (NI-RPIM) are investigated on the solution accuracy of 3D elastostatic problems. The nodal integration technique is based on Taylor series expansion and, generally, its first two terms are used. It is only applied to 2D elastostatic problems in the literature. However, in the current study, terms are used up to the 5th order and it is applied to 3D elastostatic problems. Integration domains are obtained with rectangular prisms. Three different case studies are solved with different support domain sizes and shape parameters. Their results are compared with the finite element method, RPIM with Gauss integration, and available analytical solutions. Results are discussed in detail.

Key words: NI-RPIM, nodal integration, Taylor expansion, 3D static problems

1. Introduction

Various numerical techniques have been developed for solutions of engineering problems. They provide not only support for an alternative solution to experimental analyses, but also support for fast investigation of analyzed system parameters of various combinations. However, most engineering problems have complex properties including complex shapes, time-dependent responses, and nonlinear behavior. Approximations and some simplifications are mostly used for applying numerical analysis methods properly. However, if the required conditions are not provided, the accuracy of solutions decreases.

Representation of analyzed models with mathematical descriptions and boundary conditions has a dominant effect on the accuracy of solutions. Some methods have been developed and are available in the literature. The finite element method (FEM), boundary element method (BEM), finite difference method (FDM), finite volume method (FVM), and their adaptations are widely used. They are also used in the solutions of engineering problems. Some software package programs for these methods are available, which have been mostly prepared with the FEM.

The analyzed model is divided into small elements, which are called finite elements, in the FEM. The solution of a model is executed based on these elements. Their shapes, numbers, and quality affect solution accuracy. Hence, it is required to construct a suitable FEM, which consumes most of the analysis time. If construction of FEM modeling is simplified or eliminated, the consumed time of finite element modeling is saved.

*Correspondence: kanber@gantep.edu.tr

Meshfree methods are another developing technique and mainly aim to remove the dependency of mesh construction. Some researchers have succeeded at eliminating predefined element construction by meshfree methods. Smoothed particle hydrodynamics (SPH) is one of the meshfree methods, mainly designed for solutions of astrophysical problems [1,2]. It is further adapted to use solutions of different kinds of problems. SPH is used in solutions of mechanic problems [3,4]. Besides that, different types of meshfree methods have been developed. The diffuse element method was developed to prevent requirements of mesh generation [5]. Other meshfree methods like the element-free Galerkin method [6], reproducing kernel particle method [7], meshless local Petrov–Galerkin method [8], point interpolation method (PIM) [9], and radial point interpolation method (RPIM) [10] have been developed. Radial basis functions (RBFs) are widely used in meshfree approximations. RBF is also used for developing the boundary knot method [11].

The PIM and RPIM [12] are used in the construction of boundary integral equations in BEM. The PIM and RPIM are adapted in various integration schemes. The linearly conforming point interpolation method (LC-PIM) [13], nodal integration radial point interpolation method (NI-RPIM) [14], node-based smoothed point interpolation method (NS-PIM) [15], cell-based smoothed radial point interpolation method (CS-RPIM) [16], and edge-based smoothed point interpolation method (ES-PIM) [17] are available in the literature. Most of them are used in the solutions of solid mechanics problems. The natural neighbor radial point interpolation method (NNR-PIM) is one of the meshfree methods, used for investigation of 3D solids [18] and plates [19] by using RBFs. Most of these methods allow elimination of predefined mesh dependency for construction of shape functions. However, more studies are needed for fully eliminating mesh generation for interpolation and integration.

Effects of RBF shape parameters were also studied [20–22] in the literature. It was observed that values of shape parameters can affect the results.

In the literature, Taylor approximation terms are used up to the fourth order for decreasing singularity problems [23] in the BEM and increasing accuracy [24] in finite difference calculations on arbitrary meshes. It was observed in some studies [23,24] that third order terms have better accuracy than first and second order terms. Higher order [25–27] Taylor series approximations were also recommended in some studies. The automatic Taylor expansion technique (ATET) [28] was used on Euler–Bernoulli cantilever beam problems, which includes the fifth order terms of ATET solutions. In nodal integration calculations of solid mechanics problems, second order terms can be enough for displacement calculations. However, if stress results are evaluated, it is better to use fourth order terms in some investigated cases [29] for 2D elastostatic problems. Although the method is applied and investigated for 2D cases, the usage of higher order terms of Taylor series expansion on nodal integration is limited, especially in 3D RPIM.

Hence, in this study, effects of degrees of Taylor series expansion are investigated for 3D cases with hexahedral integration cells. The results are compared with RPIM with Gauss integration, FEM (ANSYS), and available analytical results. A meshfree program is generated using NI-RPIM. This method [14] uses Taylor series expansion in nodal integration. Effect of shape parameters (α_c and q) and support domain (sd) size are also investigated. Three different case studies are examined and results are discussed in detail.

2. RPIM shape functions

Construction of shape functions is the most critical step of numerical analyses. They describe basic relationships between field nodes. Their quality can directly influence results. The usage of higher qualified shape functions

mostly increases accuracy. Different methods have been developed for construction of shape functions. The basic idea of construction of shape functions in the FEM is designed with the relationship between elements and their components. The condition of elements and components needs highly qualified properties. However, it consumes most of the analysis time. Hence, meshfree methods are an alternative way for these numerical applications.

The RPIM [10] is one of the meshfree techniques and uses the PIM [9] with radial basis functions. In this method, polynomial and basis functions are used for representation of a field function, $u(x)$, as follows:

$$u(x) = \sum_{i=1}^{n} R_i(x) \times a_i + \sum_{j=1}^{m} P_j(x) \times b_j = R^T(x) \times a + P^T(x) \times b. \tag{1}$$

$R_i(x)$ and $P_j(x)$ represent radial basis and polynomial basis functions, respectively. a_i and b_j are related constants, n is the number of field nodes in the local support domain, and m is the number of polynomial terms. Interpolations between nodes are mainly accomplished within the local support domain for each node or point of interests.

Different kinds of RBFs are available in the literature [30,31], like multiquadric (MQ), Gaussian (Exp), thin plate spline (TSP), and logarithmic radial basis functions. MQ is used [18,30] as a radial basis function in Eq. (2).

$$R_i(x) = \left(r_i^2 + (\alpha_c \times d_c)^2\right)^q \tag{2}$$

Here, d_c is the average nodal spacing near the point of interest at x, and α_c and n are two arbitrary real numbers of dimensionless parameters, which are called shape parameters. It is recommended [30,31] to use q as 1.03 and $\alpha_c \alpha_c$ as 3.00 for the MQ basis function. The radial distance is given in Eq. (3) for 3D cases. The polynomial terms are given in Eq. (4), which are mainly derived from binomial expansion.

$$r_i(x) = \sqrt{(x - x_i)^2 + (y - y_i)^2 + (z - z_i)^2} \tag{3}$$

$$p^T(x) = \left\{1, x, y, z, x^2, xy, y^2, yz, z^2, zx, ...\right\} \tag{4}$$

Interpolation is applied in a support domain for a point of interest. Different types of support domain geometries can be used, like circular, elliptical, triangular, or rectangular. A circular local support domain is used and its covered area is given by the radius of the circle (d_s), which is given in Eq. (5):

$$d_s = \alpha_s \times d_c, \tag{5}$$

where d_c is the average nodal spacing and α_s is a positive real number of dimensionless size of the local support domain. Its value [18,30] is commonly used between 2.00 and 3.00. The unknown constants of the field function of a_i and b_j in Eq. (1) can be determined by enforcing the field function passing through all n field nodes in the local support domain. At the kth point or the last point in a local support domain, the field function can be written as:

$$u(x_k, y_k, z_k) = \sum_{i=1}^{n} R_i(x_k, y_k, z_k) \times a_i + \sum_{j=1}^{m} P_j(x_k, y_k, z_k) \times b_j \quad k = 1, 2, ..n. \tag{6}$$

The matrix form of the above equation can be expressed as:

$$U_e = R_q \times a + P_m \times b = \{u_1 u_2 ... u_n\}^T, \tag{7}$$

where U_e is the vector of function values at the nodes in the local support domain. R_q is the moment matrix and P_m is the polynomial moment matrix [30], which are given in Eqs. (8) and (9), respectively.

$$R_q = \begin{bmatrix} R_1(r_1) & R_2(r_1) & \dots & R_n(r_1) \\ R_1(r_2) & R_2(r_2) & \dots & R_n(r_2) \\ \dots & \dots & \dots & \dots \\ R_1(r_n) & R_2(r_n) & \dots & R_n(r_n) \end{bmatrix}_{(n\times n)} \tag{8}$$

$$P_m = \begin{bmatrix} 1 & x_1 & y_1 & z_1 & \cdots & P_m(r_1) \\ 1 & x_2 & y_2 & z_2 & \cdots & P_m(r_2) \\ \dots & \dots & \dots & \cdots & \cdots & \dots \\ 1 & x_n & y_n & z_n & \cdots & P_m(r_n) \end{bmatrix}_{(n\times m)} \tag{9}$$

a is the vector of unknown coefficients for RBF and b is the vector of unknown coefficients for polynomial basis functions. They are given in Eqs. (10) and (11).

$$a^T = \{a_1 a_2 ... a_n\} \tag{10}$$

$$b^T = \{b_1 b_2 ... b_n\} \tag{11}$$

For solutions of the field function, the unknown parameter a in Eq. (7) must satisfy the polynomial function:

$$\sum_{i=1}^{n} p_j(x_i) \times a_i = P_m^T \times a = 0 \tag{12}$$

j = 1,2,..,m.

Combination of Eq. (7) and Eq. (1) yields the following equations in matrix form:

$$\tilde{U}_e = \begin{bmatrix} U_e \\ 0 \end{bmatrix} = \begin{bmatrix} R_q & P_m \\ P_m^T & 0 \end{bmatrix} \begin{Bmatrix} a \\ b \end{Bmatrix} = G \times a_0, \tag{13}$$

where

$$\tilde{U}_e = \begin{bmatrix} U_e \\ 0 \end{bmatrix} = \{a_1 a_2 ... a_n 00...0\}^T. \tag{14}$$

A unique solution is obtained if the inverse of matrix G exists:

$$a_0 = \begin{Bmatrix} a \\ b \end{Bmatrix} = G^{-1} \times \tilde{U}_e. \tag{15}$$

Substituting Eq. (15) into Eq. (1), interpolation with respect to the field function can be expressed as:

$$u(x) = \left\{R^T(x) \times P^T(x)\right\} \times G^{-1} \times \tilde{U}_e = \tilde{\phi}(x) \times \tilde{U}_e. \tag{16}$$

Finally, RPIM shape functions for the corresponding n field nodes can be obtained as [18,30]:

$$\phi^T(x) = \{\phi_1(x)\,\phi_2(x)\ldots\phi_n(x)\}. \tag{17}$$

The approximation function can be written as:

$$u(x) = \phi^T(x) \times U_e = \sum_{i=1}^{n} \phi_i \times u_i. \tag{18}$$

The derivatives of $u(x)$ can be easily obtained as:

$$u_{i,k}(x) = \phi^T_{,k}(x) \times U_e, \tag{19}$$

where k denotes the coordinates x, y, or z. Partial differentiation is taken with respect to that defined coordinated by k.

3. Nodal integration based on Taylor series expansion

The approximated solution must be adapted to the equilibrium equation. The equilibrium equation is given in Eq. (20), which is valid in the domain. Applied natural and essential boundary conditions [14,30] are given in Eqs. (21) and (22), respectively.

$$L^T \times \sigma + b = 0 \tag{20}$$

$$\sigma \cdot n = \bar{t}\,\text{on}\,\tau_i \tag{21}$$

$$u = \bar{u}\,\text{on}\,\tau_u \tag{22}$$

L^T is the differential operator [30], σ is the stress vector, u is the displacement vector, b is the body force vector, $\bar{t}$ is prescribed traction on the natural boundaries, $\bar{u}$ is prescribed displacement on the essential boundaries, and n is the vector of unit outward normal on the natural boundary. They are given in Eqs. (23), (24), (25), and (26), respectively.

$$L^T = \begin{bmatrix} \partial/\partial x & 0 & 0 & 0 & \partial/\partial z & \partial/\partial y \\ 0 & \partial/\partial y & 0 & \partial/\partial z & 0 & \partial/\partial x \\ 0 & 0 & \partial/\partial z & \partial/\partial y & \partial/\partial x & 0 \end{bmatrix} \tag{23}$$

$$\sigma^T = \begin{bmatrix} \sigma_{xx} & \sigma_{yy} & \sigma_{zz} & \tau_{yz} & \tau_{xz} & \tau_{xy} \end{bmatrix} \tag{24}$$

$$u = \begin{bmatrix} u \\ v \\ w \end{bmatrix} \tag{25}$$

$$b = \begin{bmatrix} b_x \\ b_y \\ b_z \end{bmatrix} \tag{26}$$

The equilibrium equation (Eq. (20)) can be defined as in Galerkin weak formulation in Eq. (27):

$$\int (L \times \delta u)^T \times (D \times L \times u)\, d\Omega - \int \left(\delta u^T \times b\right) d\Omega - \int \left(\delta u^T \times t\right) d\Gamma = 0. \tag{27}$$

The D matrix is a material coefficient matrix and it is given for isotropic solids as:

$$D = \frac{E \times (1-\nu)}{(1+\nu) \times (1-2\nu)} \times \begin{bmatrix} 1 & \frac{\nu}{1-\nu} & \frac{\nu}{1-\nu} & 0 & 0 & 0 \\ \frac{\nu}{1-\nu} & 1 & \frac{\nu}{1-\nu} & 0 & 0 & 0 \\ \frac{\nu}{1-\nu} & \frac{\nu}{1-\nu} & 1 & 0 & 0 & 0 \\ 0 & 0 & 0 & \frac{1-2\nu}{2\times(1-\nu)} & 0 & 0 \\ 0 & 0 & 0 & 0 & \frac{1-2\nu}{2\times(1-\nu)} & 0 \\ 0 & 0 & 0 & 0 & 0 & \frac{1-2\nu}{2\times(1-\nu)} \end{bmatrix}, \tag{28}$$

where E is the Young modulus and ν is Poisson's ratio [30]. When substituting the approximated Eq. (18), into Eq. (27), we have:

$$K \times u = f, \tag{29}$$

where:

$$K_{ij} = \int B_i^T \times D \times B_j d\Omega, \tag{30}$$

$$f_i = \int \phi_i \times t d\Gamma + \int \phi_i \times b d\Omega, \tag{31}$$

$$B_i = \begin{bmatrix} \phi_{i,x} & 0 & 0 \\ 0 & \phi_{i,y} & 0 \\ 0 & 0 & \phi_{i,z} \\ 0 & \phi_{i,z} & \phi_{i,y} \\ \phi_{i,z} & 0 & \phi_{i,x} \\ \phi_{i,y} & \phi_{i,x} & 0 \end{bmatrix}. \tag{32}$$

Series are widely used in mathematical operations, especially in numerical studies. An unknown value of a valid function can be estimated with a known value with series operations. Different kinds of series are available in the literature. One of the series is the Taylor series and it is widely used in computational fluid dynamics with respect to the finite difference method (FDM). An example of value estimation from x_0 to $x_0 + h$ can be defined as serial expansion of the value of functions and it is given in Eq. (33). R_n is the total error between

values of $f(x_0+h)$ and its Taylor expansion results. In general, the degree of used terms in the FDM increases the accuracy.

$$f\left(x_0+h\right)=f\left(x_0\right)+\frac{f'\left(x_0\right)}{1!}\times h+\frac{f''\left(x_0\right)}{2!}\times h^2+\frac{f'''\left(x_0\right)}{3!}\times h^3+...+\frac{f^n\left(x_0\right)}{n!}\times h^n+R_n \tag{33}$$

Taylor series expansion was used in nodal integration in [14]. Eq. (29) represents the stiffness matrix and will be used as an approximate function $f\left(x,y,z\right)$, which is given in Eq. (34).

$$\begin{aligned} f\left(x,y,z\right) \;=\; & f\left(x_0,y_0,z_0\right)+\left(x-x_0\right)\times\tfrac{\partial f(x_0,y_0,z_0)}{\partial x}+\left(y-y_0\right)\times\tfrac{\partial f(x_0,y_0,z_0)}{\partial y} \\ & +\left(z-z_0\right)\times\tfrac{\partial f(x_0,y_0,z_0)}{\partial z}+\tfrac{1}{2!}\times\left(x-x_0\right)^2\times\tfrac{\partial^2 f(x_0,y_0,z_0)}{\partial x^2}+\tfrac{1}{2!}\times 2 \\ & \times\left(x-x_0\right)\times\left(y-y_0\right)\times\tfrac{\partial^2 f(x_0,y_0,z_0)}{\partial x\partial y}+\tfrac{1}{2!}\times\left(y-y_0\right)^2\times\tfrac{\partial^2 f(x_0,y_0,z_0)}{\partial y^2} \\ & +\tfrac{1}{2!}\times 2\times\left(y-y_0\right)\times\left(z-z_0\right)\times\tfrac{\partial^2 f(x_0,y_0,z_0)}{\partial y\partial z}+\tfrac{1}{2!}\times\left(z-z_0\right)^2 \\ & \times\tfrac{\partial^2 f(x_0,y_0,z_0)}{\partial z^2}+\tfrac{1}{2!}\times 2\times\left(z-z_0\right)\times\left(x-x_0\right)\times\tfrac{\partial^2 f(x_0,y_0,z_0)}{\partial z\partial x}+\tfrac{1}{3!} \\ & \times\left(x-x_0\right)^3\times\tfrac{\partial^3 f(x_0,y_0,z_0)}{\partial x^3}+\tfrac{1}{3!}\times\left(y-y_0\right)^3\times\tfrac{\partial^3 f(x_0,y_0,z_0)}{\partial y^3}+\tfrac{1}{3!} \\ & \times\left(z-z_0\right)^3\times\tfrac{\partial^3 f(x_0,y_0,z_0)}{\partial z^3}+\tfrac{1}{3!}\times 3\times\left(x-x_0\right)^2\times\left(y-y_0\right)\times\tfrac{\partial^3 f(x_0,y_0,z_0)}{\partial x^2\partial y}+... \end{aligned} \tag{34}$$

The nodal integration of Eq. (34) can be written as in Eq. (35).

$$\begin{aligned} \int f\left(x,y,z\right)d\Omega \;=\; & \int\Big(f\left(x_0,y_0,z_0\right)+\left(x-x_0\right)\times\tfrac{\partial f(x_0,y_0,z_0)}{\partial x}+\left(y-y_0\right) \\ & \times\tfrac{\partial f(x_0,y_0,z_0)}{\partial y}+\left(z-z_0\right)\times\tfrac{\partial f(x_0,y_0,z_0)}{\partial z}+\tfrac{1}{2!}\times\left(x-x_0\right)^2\times\tfrac{\partial^2 f(x_0,y_0,z_0)}{\partial x^2} \\ & +\tfrac{1}{2!}\times 2\times\left(x-x_0\right)\times\left(y-y_0\right)\times\tfrac{\partial^2 f(x_0,y_0,z_0)}{\partial x\partial y}+\tfrac{1}{2!}\times\left(y-y_0\right)^2\times\tfrac{\partial^2 f(x_0,y_0,z_0)}{\partial y^2} \\ & +\tfrac{1}{2!}\times 2\times\left(y-y_0\right)\times\left(z-z_0\right)\times\tfrac{\partial^2 f(x_0,y_0,z_0)}{\partial y\partial z}+\tfrac{1}{2!}\times\left(z-z_0\right)^2\times\tfrac{\partial^2 f(x_0,y_0,z_0)}{\partial z^2} \\ & +\tfrac{1}{2!}\times 2\times\left(z-z_0\right)\times\left(x-x_0\right)\times\tfrac{\partial^2 f(x_0,y_0,z_0)}{\partial z\partial x}+\tfrac{1}{3!}\times\left(x-x_0\right)^3\times\tfrac{\partial^3 f(x_0,y_0,z_0)}{\partial x^3} \\ & +\tfrac{1}{3!}\times\left(y-y_0\right)^3\times\tfrac{\partial^3 f(x_0,y_0,z_0)}{\partial y^3}+\tfrac{1}{3!}\times\left(z-z_0\right)^3\times\tfrac{\partial^3 f(x_0,y_0,z_0)}{\partial z^3}+\tfrac{1}{3!}\times 3\times \\ & +\left(x-x_0\right)^2\times\left(y-y_0\right)\times\tfrac{\partial^3 f(x_0,y_0,z_0)}{\partial x^2\partial y}+...\Big)d\Omega \end{aligned} \tag{35}$$

If Eq. (35) is arranged, the following form can be obtained.

$$\begin{aligned} \int f\left(x,y,z\right)d\Omega \;=\; & \int f\left(x_0,y_0,z_0\right)d\Omega+\int\left(x-x_0\right)\times\tfrac{\partial f(x_0,y_0,z_0)}{\partial x}d\Omega+\int\left(y-y_0\right) \\ & \times\tfrac{\partial f(x_0,y_0,z_0)}{\partial y}d\Omega+\int\left(z-z_0\right)\times\tfrac{\partial f(x_0,y_0,z_0)}{\partial z}d\Omega+\int\tfrac{1}{2!}\times\left(x-x_0\right)^2 \\ & \times\tfrac{\partial^2 f(x_0,y_0,z_0)}{\partial x^2}d\Omega+\int\tfrac{1}{2!}\times 2\times\left(x-x_0\right)\times\left(y-y_0\right)\times\tfrac{\partial^2 f(x_0,y_0,z_0)}{\partial x\partial y}d\Omega \\ & +\int\tfrac{1}{2!}\times\left(y-y_0\right)^2\times\tfrac{\partial^2 f(x_0,y_0,z_0)}{\partial y^2}d\Omega+\int\tfrac{1}{2!}\times 2\times\left(y-y_0\right)\times\left(z-z_0\right) \\ & \times\tfrac{\partial^2 f(x_0,y_0,z_0)}{\partial y\partial z}d\Omega+\int\tfrac{1}{2!}\times\left(z-z_0\right)^2\times\tfrac{\partial^2 f(x_0,y_0,z_0)}{\partial z^2}d\Omega+\int\tfrac{1}{2!}\times 2 \\ & \times\left(z-z_0\right)\times\left(x-x_0\right)\times\tfrac{\partial^2 f(x_0,y_0,z_0)}{\partial z\partial x}d\Omega+\int\tfrac{1}{3!}\times\left(x-x_0\right)^3\times\tfrac{\partial^3 f(x_0,y_0,z_0)}{\partial x^3}d\Omega+... \end{aligned} \tag{36}$$

$$\begin{aligned}\int f(x,y,z)d\Omega &= f(x_0,y_0,z_0)\times\int 1d\Omega + f_x(x_0,y_0,z_0)\times\int(x-x_0)\,d\Omega \\ &+f_y(x_0,y_0,z_0)\times\int(y-y_0)d\Omega + f_z(x_0,y_0,z_0)\times\int(z-z_0)\,d\Omega \\ &+f_{xx}(x_0,y_0,z_0)\times\tfrac{1}{2!}\times\int(x-x_0)^2d\Omega + f_{xy}(x_0,y_0,z_0) \\ &\times\int(x-x_0)\times(y-y_0)d\Omega+\ldots\end{aligned} \tag{37}$$

In Eq. (37), $x-x_0$ represents Δx, $y-y_0$ represents Δy, and $z-z_0$ represents Δz. The distance is calculated from the midpoint of the Taylor cell and field nodes. $d\Omega$ is equal to the volume of the Taylor integration cell. Each Taylor integration cell for each field node includes a volume that does not interact with other field nodes of Taylor integration cells.

4. Solutions and discussion

Effects of Taylor expansion terms in nodal integration are investigated by using a program that is developed in FORTRAN. The code is written based on the studies in the literature [14,30]. A computer with processor speed of 2.4 GHz and memory capacity of 3 GB is used in the analyses. In all cases, in order to concentrate on the effect of Taylor series terms, the effects of RPIM shape parameters are reduced by selecting high numbers of nodes in the models.

Three different case studies are examined with different boundary conditions. They are selected to test the nodal integration algorithm. Although authors previously used isoparametric transformation for complex geometries [32], in this study, we try to observe the performance of orders of Taylor terms on basic integration operations without using isoparametric transformation. A simply supported beam with distributed load, a torsion bar, and an L-shaped beam under uniform load are examined. The simply supported beam with distributed load is given in Figure 1a. The torsion bar is given in Figure 1b and the L-shaped beam under uniform load is given in Figure 1c. A linear elastic material is used with a Young modulus of 200 GPa and Poisson's ratio of 0.0. The selection of Poisson's ratio as 0.0 is aimed for providing similar conditions to analytical solutions.

A bar/beam with square section of 0.1 m $\times$ 0.1 m and length of 1.00 m is used in case I and case II. The L-shaped beam has a length of 1.00 m in the x-direction and 0.5 m in the z-direction. A force couple is used for applied torque in case I, which is equal to 75 Nm. Applied distributed load is 22,500 $\mathrm{N/m^2}$ in case II. Uniformly varying load is used as 2250 N/m in case III. Node distributions are the same in the FEM and meshfree models.

SOLID 185 finite elements are used in FEM models, which have 8 nodes at the edges. The ANSYS 14 software package program is used in the FEM preprocessor, solution, and postprocessor steps. An element length of 0.05 m is selected in models. The FEM of the simply supported beam (case II) is given in Figure 2a and the L-shaped beam (case III) is given in Figure 2b. The meshfree model of the simply supported beam is given in Figure 3a, which has 189 nodes. The meshfree model of the L-shaped beam (case III) is given in Figure 3b, which has 270 nodes. The FEM and meshfree models of case I have 6561 nodes with an element length of 0.0125 m.

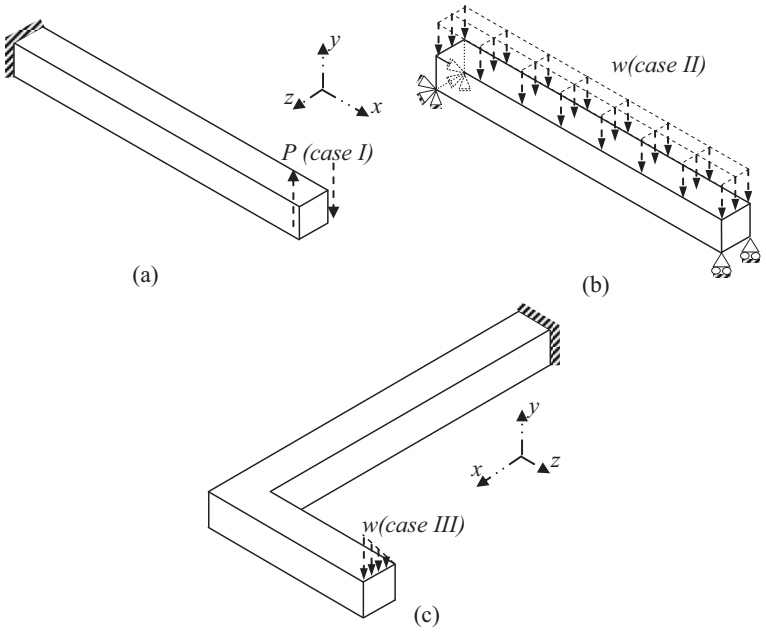

Figure 1. The used models in the analyses and boundary conditions: a) bar under torsion (case I), b) simply supported beam problem with distributed loaded (case II), c) L-shaped beam under uniformly varying load (case III).

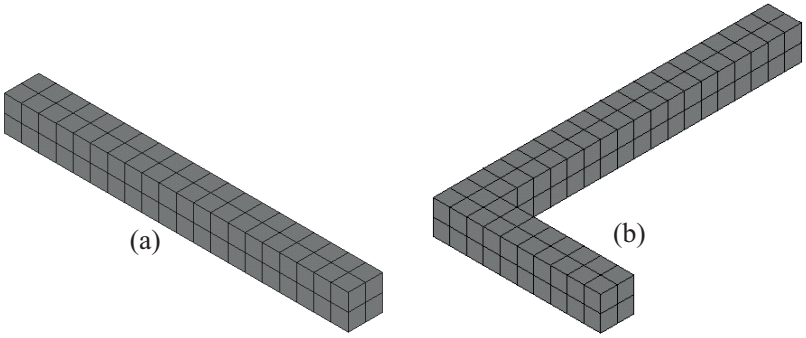

Figure 2. FEM models of analyzed cases: a) beam for case II, b) L-shaped beam for case III.

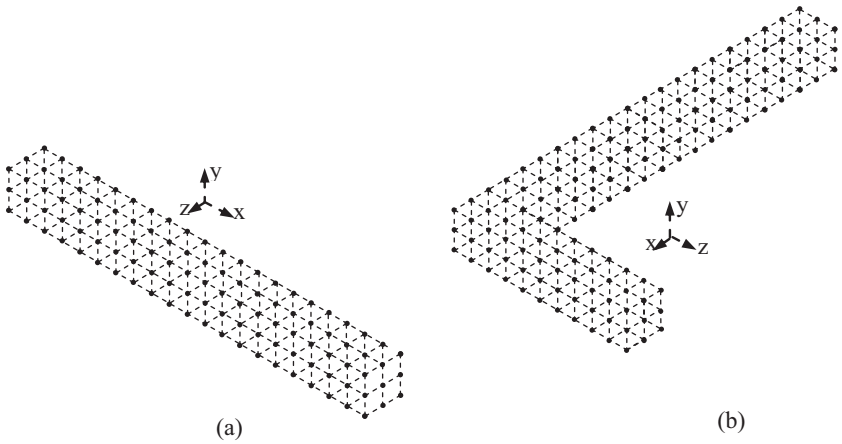

Figure 3. Meshfree models of analyzed cases: a) beam for case II, b) L-shaped beam for case III.

The vertical deflection of the simply supported beam [33] with distributed loading (case II) is given as follows:

$$y = -\frac{w}{24 \times E \times I} \times \left(x^4 - 2 \times L \times x^3 - L^3 \times x\right), \tag{38}$$

where w is applied distributed load and I represents inertia of the beam. E is Young's modulus and x is the distance from a fixed support location. L is the total length of the beam. Its bending stress at the upper and lower surfaces is given as:

$$\sigma = \frac{M \times c}{I}, \tag{39}$$

where c is the distance between the upper surface and neutral axis of the beam.

The twist angle (Φ) and maximum shear stress ($\tau_{\max}$) in a torsion bar (case I) are analytically given [33,34] as follows:

$$\Phi = \frac{T \times c}{c_2 \times a \times b^3 \times G}, \tag{40}$$

$$\tau_{\max} = \frac{T}{c_1 \times a \times b^2}, \tag{41}$$

where T is applied torque and a and b are height and width of the beam, which are equal to 0.1 m and 0.1 m. c_1 and c_2 are constants for noncircular torsion of members, which are equal to 0.208 and 0.1406 with respect to a square cross-section.

α_c is used as 3.00, support domain size is used as 1.30, and q is used as 1.03 as a default parameter in the solutions of RPIM methods.

4.1. Torsion bar

Torsion of a noncircular bar with a square cross-section is investigated. Twist angle results are taken from the side surface of the bar, where the maximum shear stresses occur. Shear stress results are taken from the upper surface at the mid-length of the bar.

Twist angle results (case I) are given in Figures 4 and 5 for nodal and Gauss integrations. It is observed that the 1st terms of nodal integration include serious errors with respect to analytical solution. The 2nd, 3rd, 4th, and 5th orders of nodal integration results have similar characteristics with analytical results, but the FEM results are closer than RPIM to nodal integration results. RPIM with Gauss integrations gives similar results as 2nd and higher order terms' results of nodal integration in Figure 5. The number of sampling points has no effect on the results for this case.

Shear stress results are compared in Table 1. The 2nd and further order terms in nodal integration and Gauss integration with 3 $\times$ 3 and 4 $\times$ 4 sampling points give better results than the FEM compared to the analytical solution. Gauss integration with 3 $\times$ 3 sampling points gives the closest results to the analytical results. The 1st order terms of nodal integration and 2 $\times$ 2 sampling points of Gauss integration results include less sensitivity.

The effects of α_c on twist angle results (case I) are given in Figures 6 and 7. The α_c values of 1.00, 3.00, and 5.00 have the same results for the solutions of Gauss integration. α_c values of 7.00 and 9.00 cause failure of shape function construction. α_c values of 1.00, 3.00, 7.00, and 9.00 in nodal integration have similar results and enough accuracy with the analytical solution. The α_c value of 5.00 in nodal integration has the least accuracy.

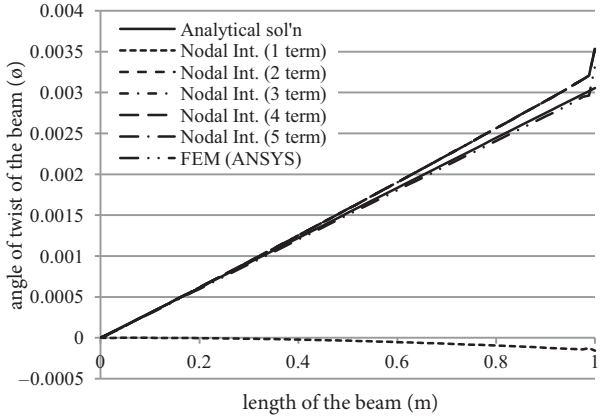

Figure 4. Comparison of twist angle results of a noncircular bar under torsion (case I) for analytical, FEM, and nodal int. techniques.

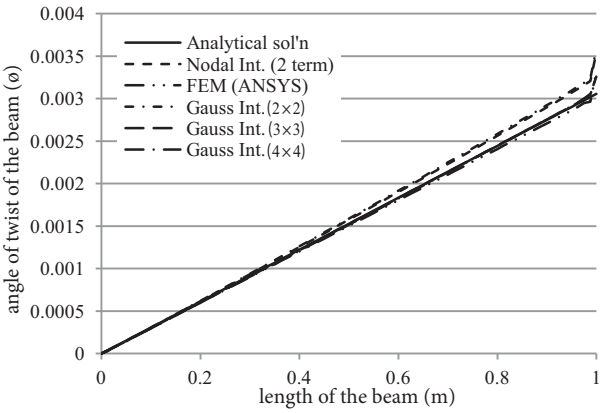

Figure 5. Comparison of twist angle results of a noncircular bar under torsion (case I) for analytical, Gauss, and nodal int. (2 terms) techniques.

Table 1. Comparison of shear stress results of a noncircular bar under torsion (case I) for analytical, FEM, and nodal integration techniques.

Solution technique	τ_{xy} (kPa)
FEM (ANSYS)	352.19
Nodal int. (1 term)	388.90
Nodal int. (2 terms)	366.11
Nodal int. (3 terms)	365.96
Nodal int. (4 terms)	366.04
Nodal int. (5 terms)	366.04
Gauss int. (2×2)	369.88
Gauss int. (3×3)	359.47
Gauss int. (4×4)	354.01
Analytical solution	360.57

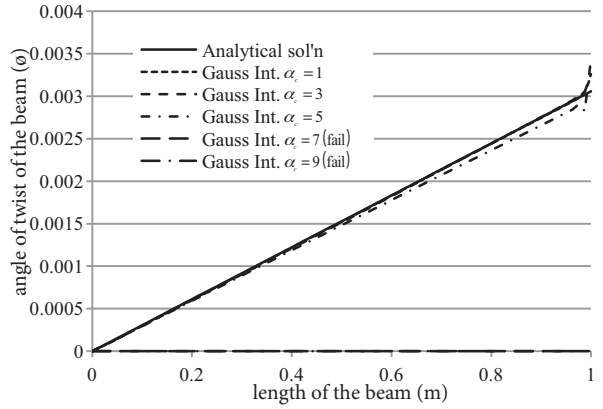

Figure 6. Comparison of effect of α_c on twist angle results of a noncircular bar under torsion (case I) for 4×4 Gauss int.

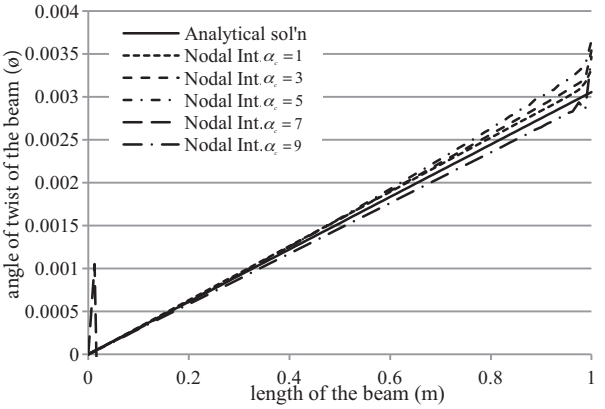

Figure 7. Comparison of effect of α_c on twist angle results of a noncircular bar under torsion (case I) for nodal int. (2 terms).

Effects of support domain size are given in Figures 8 and 9 for case I. Support domain size of $6.5 \times L/100$ has similar results as the analytical solution in Gauss integration. The usage of support domain size of $7.5 \times L/100$ decreases accuracy. Further increments of support domain sizes cannot satisfy construction of shape functions and fail. Results of different support domain sizes have similar results and enough accuracy without $1.5 \times L/10$ in nodal integration.

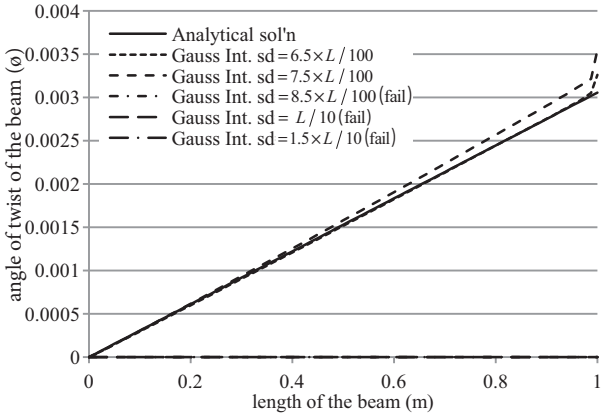

Figure 8. Comparison of effect of sd on twist angle results of a noncircular bar under torsion (case I) for 4×4 Gauss int.

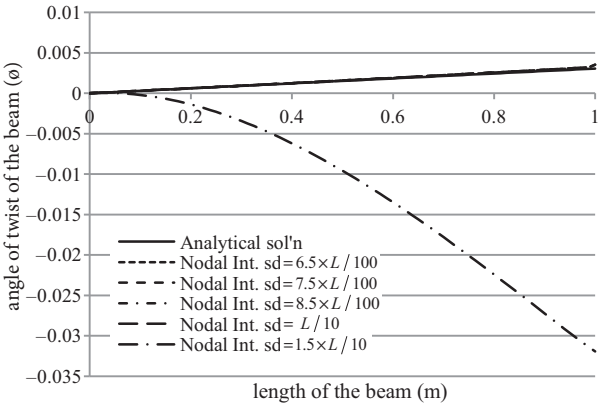

Figure 9. Comparison of effect of sd on twist angle results of a noncircular bar under torsion (case I) for nodal int. (2 terms).

Effects of q on twist angle results are given in Figures 10 and 11. q values of 0.5 and 0.98 cause failure in the construction of shape functions in RPIM with Gauss integration. q values of 0.7 and 1.03 have better accuracy than 1.30. In nodal integration results, all q values have high fluctuations when a different value from 1.03 is used.

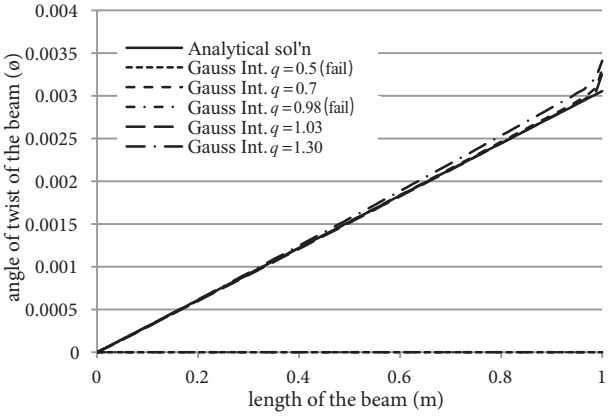

Figure 10. Comparison of effect of q on twist angle results of a noncircular bar under torsion (case I) for 4×4 Gauss int.

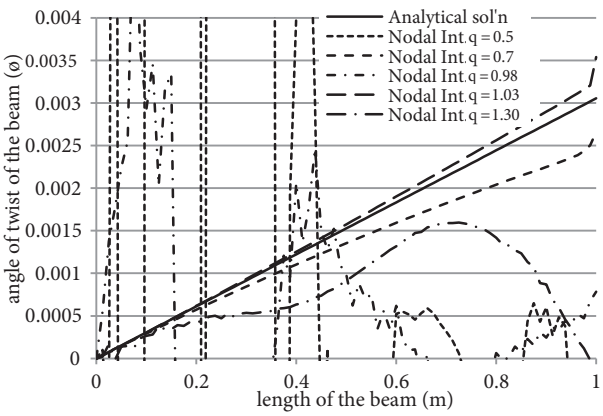

Figure 11. Comparison of effect of q on twist angle results of a noncircular bar under torsion (case I) for nodal int. (2 terms).

Effects of α_c, sd, and q on shear stress results (case I) are given in Tables 2, 3, and 4, respectively. Analytical solution results of shear stress are equal to 360.57 kPa for Tables 2, 3, and 4. α_c values of 7.00 and 9.00; sd values of $8.5 \times L/100$, $L/10$, and $1.5 \times L/10$; and q values of 0.5 and 0.98 in Gauss integration cannot

satisfy construction of shape functions and fail. The α_c value of 1.00 has the closest results. When increasing its value, accuracy decreases. sd values of $6.5 \times L/100$ and $7.5 \times L/100$ have similar accuracy. Different values of q results are close enough to analytical solution. When nodal integration results are discussed, the α_c value of 5.00 has the closest result to the analytical solution. Other results of α_c values have less accuracy, especially the α_c value of 7.00. All results of sd values are the same without the sd value of $1.5 \times L/10$. Results of the highest sd value have less accuracy. q values of 0.7 and 1.03 have good accuracy. However, other q values, especially the q value of 0.98, have wrong results.

Table 2. Comparison of effect of α_c on shear stress results of a noncircular bar under torsion (case I) for nodal integration (2 terms) and 4×4 Gauss integration.

Effect of α_c	τ_{xy} (kPa)	τ_{xy} (kPa)	Effect of α_c
Nodal int. ($\alpha_c = 1$)	379.95	362.64	Gauss int. ($\alpha_c = 1$)
Nodal int. ($\alpha_c = 3$)	366.11	354.01	Gauss int. ($\alpha_c = 3$)
Nodal int. ($\alpha_c = 5$)	357.56	350.63	Gauss int. ($\alpha_c = 5$)
Nodal int. ($\alpha_c = 7$)	681.29	-	Gauss int. ($\alpha_c = 7$)
Nodal int. ($\alpha_c = 9$)	344.64	-	Gauss int. ($\alpha_c = 9$)

Table 3. Comparison of effect of sd on shear stress results of a noncircular bar under torsion (case I) for nodal integration (2 terms) and 4×4 Gauss integration.

Effect of sd	τ_{xy} (kPa)	τ_{xy} (kPa)	Effect of sd
Nodal int. (sd = $6.5 \times L/100$)	366.11	354.01	Gauss int. (sd = $6.5 \times L/100$)
Nodal int. (sd = $7.5 \times L/100$)	366.11	366.93	Gauss int. (sd = $7.5 \times L/100$)
Nodal int. (sd = $8.5 \times L/100$)	366.11	-	Gauss int. (sd = $8.5 \times L/100$)
Nodal int. (sd = $L/10$)	366.11	-	Gauss int. (sd = $L/10$)
Nodal int. (sd = $1.5 \times L/10$)	370.82	-	Gauss int. (sd = $1.5 \times L/10$)

Table 4. Comparison of effect of q on shear stress results of a noncircular bar under torsion (case I) for nodal integration (2 terms) and 4×4 Gauss integration.

Effect of q	τ_{xy} (kPa)	τ_{xy} (kPa)	Effect of q
Nodal int. ($q = 0.5$)	176.78	-	Gauss int. ($q = 0.5$)
Nodal int. ($q = 0.7$)	356.05	357.75	Gauss int. ($q = 0.7$)
Nodal int. ($q = 0.98$)	-796.27	-	Gauss int. ($q = 0.98$)
Nodal int. ($q = 1.03$)	366.11	354.01	Gauss int. ($q = 1.03$)
Nodal int. ($q = 1.30$)	80.77	363.03	Gauss int. ($q = 1.30$)

4.2. Simply supported beam

Effects of different solution techniques are given in Figures 12 and 13 for case II. The usage of only 1 term of Taylor series expansion in nodal integration gives less accurate results with respect to the analytical solution. However, using more than one term in nodal integration rapidly provides accuracy, which has greater conformity with the analytical solution than the FEM (ANSYS). Results of two or more terms in nodal integration show similar characteristics. Gauss integration results are also compatible with the analytical solution.

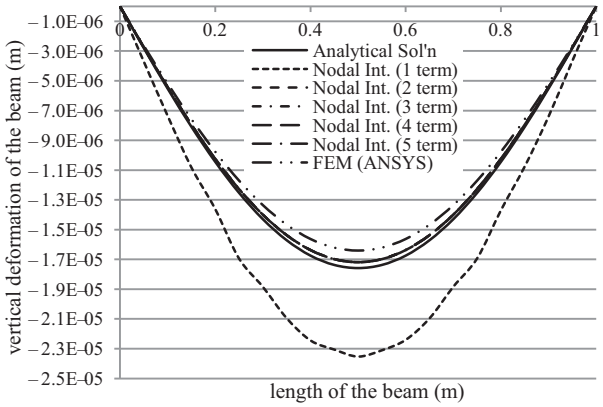

Figure 12. Comparison of vertical deformation results of distributed loaded simply supported beam (case II) for analytical, FEM, and nodal int. techniques.

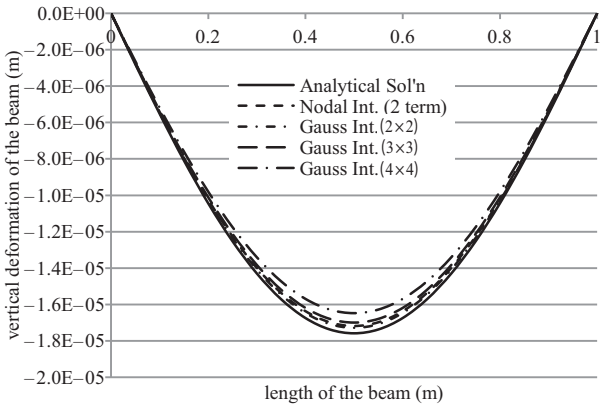

Figure 13. Comparison of vertical deformation results of distributed loaded simply supported beam (case II) for analytical, Gauss, and nodal int. (2 terms) techniques.

Bending stress results are given in Figures 14 and 15 for the simply supported beam solution. Results of the first term in nodal integration do not provide accuracy and include high fluctuations, but usage of two or more terms in nodal integration provides accuracy with respect to analytical solution. Gauss integration results have similar characteristics with second term results of nodal integration.

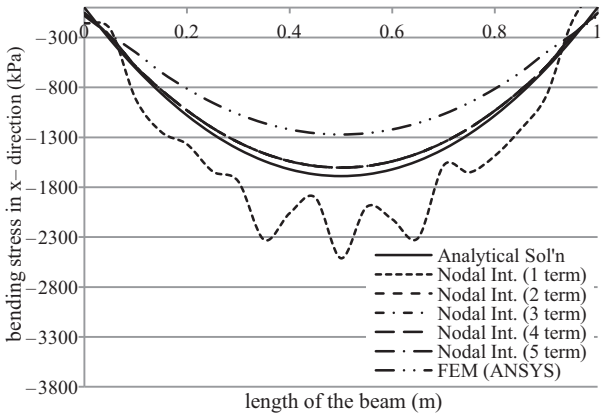

Figure 14. Comparison of bending stress results of distributed loaded simply supported beam (case II) for analytical, FEM, and nodal int. techniques.

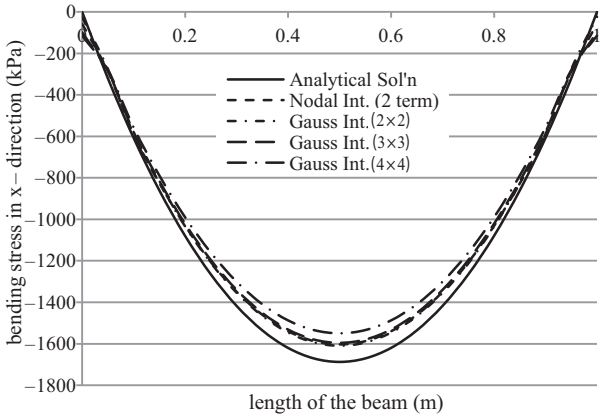

Figure 15. Comparison of bending stress results of distributed loaded simply supported beam (case II) for analytical, Gauss, and nodal int. (2 terms) techniques.

Effects of α_c on bending stress results of the simply supported beam are given in Figures 16 and 17. It is observed that α_c values of 1.00, 3.00, 5.00, and 9.00 have the same values in Gauss integration results. However, results of an α_c value of 7.00 are only different than other values of α_c results and include less accuracy. Similar responses of α_c values occur in nodal integration results. However, results of α_c values include greater deformation values than the analytical solution. In Gauss integration, deformation results are less than analytical solution.

Effects of support domain size are given on bending stress results in Figures 18 and 19. Results of an sd value of $6.5 \times L/100$ are compatible with the analytical solution in Gauss integration results. Increasing support domain size to $7.5 \times L/100$ and $8.5 \times L/100$ increases accuracy, but larger support domain sizes of

$L/10$ and $1.5 \times L/10$ decrease the accuracy of the solution. The same results of various support domain sizes occur in nodal integration.

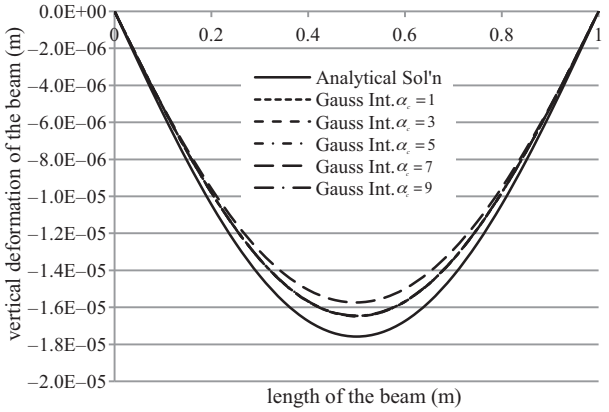

Figure 16. Comparison of effect of α_c on vertical deformation results of distributed loaded simply supported beam (case II) for 4×4 Gauss int.

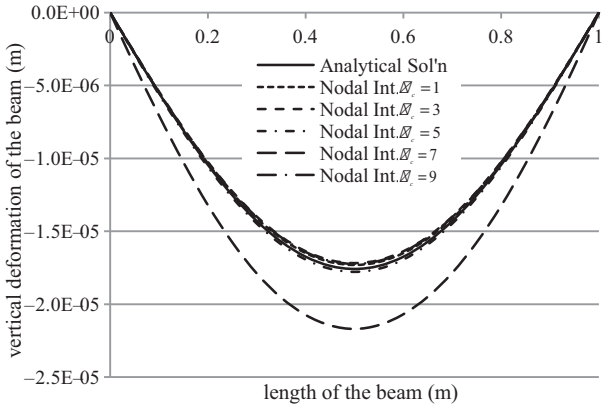

Figure 17. Comparison of effect of α_c on vertical deformation results of distributed loaded simply supported beam (case II) for nodal int. (2 terms).

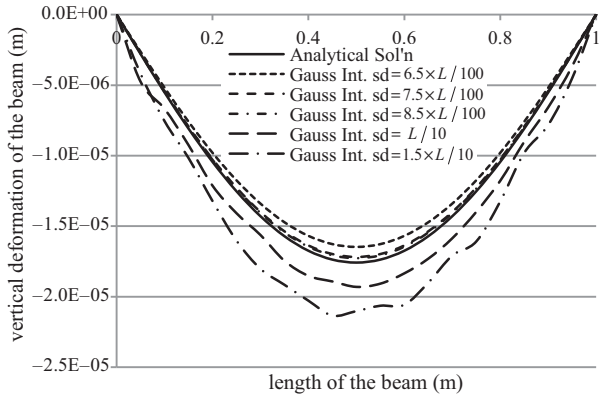

Figure 18. Comparison of effect of sd on vertical deformation results of distributed loaded simply supported beam (case II) for 4×4 Gauss int.

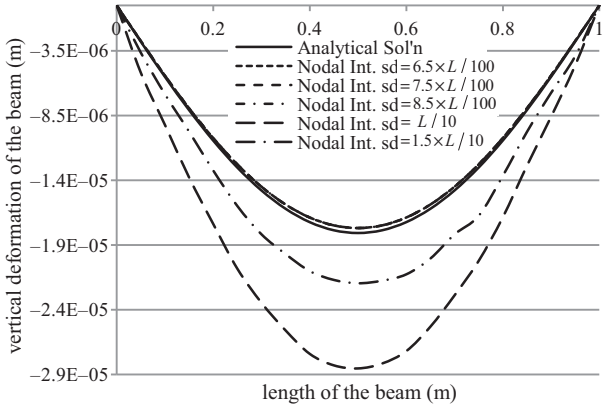

Figure 19. Comparison of effect of sd on vertical deformation results of distributed loaded simply supported beam (case II) for nodal int. (2 terms).

Effects of q on deformation results of the simply supported beam (case II) are given in Figures 20 and 21. q does not have any effect on Gauss integration results. Various q values have no effect in nodal integration without a q value of 0.98. A q value of 0.98 decreases the accuracy of the solution.

Results of bending stress distribution (case II) for various α_c values are given in Figures 22 and 23. It is observed that results of α_c values of 1.00, 3.00, 5.00, and 9.00 have nearly the same result in Gauss integration, but the result of an α_c value of 7.00 has high fluctuations and cannot satisfy accuracy. The same α_c responses are available in nodal integration. However, an α_c value of 5.00 gives the best responses in simply supported beam analyses.

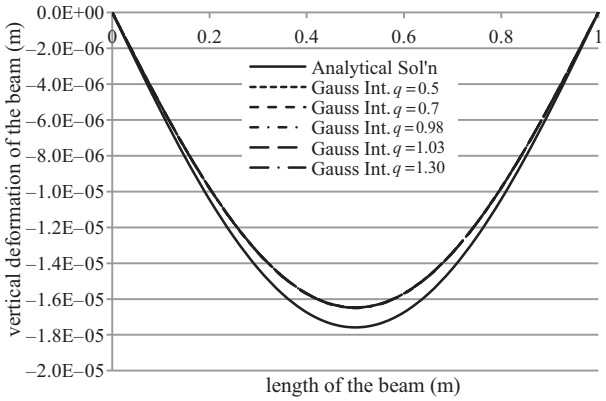

Figure 20. Comparison of effect of q on vertical deformation results of distributed loaded simply supported beam (case II) for 4×4 Gauss int.

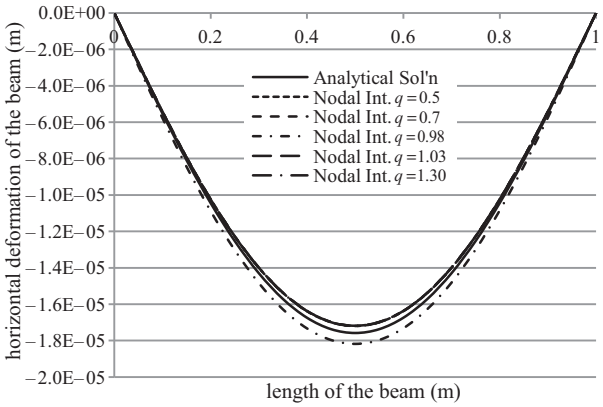

Figure 21. Comparison of effect of q on vertical deformation results of distributed loaded simply supported beam (case II) for nodal int. (2 terms).

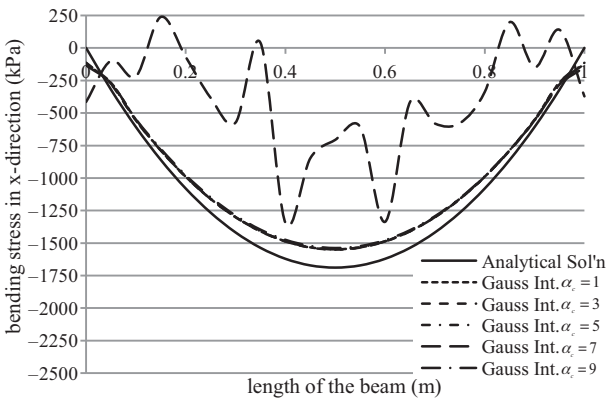

Figure 22. Comparison of effect of α_c on bending stress results of distributed loaded simply supported beam (case II) for 4×4 Gauss int.

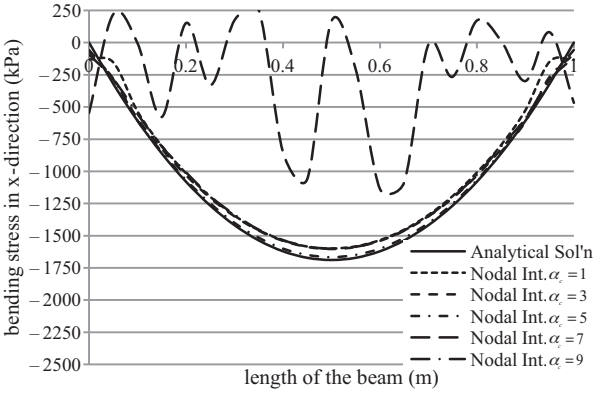

Figure 23. Comparison of effect of α_c on bending stress results of distributed loaded simply supported beam (case II) for nodal int. (2 terms).

Effect of support domain sizes on bending stress results are given in Figures 24 and 25 for case II. sd sizes of $7.5 \times L/100$ and $8.5 \times L/100$ have the highest accuracy in the results of Gauss integration, but sd sizes of $7.5 \times L/100$ also satisfy the required accuracy with respect to the analytical solution. Results of sd sizes of $L/10$ and $1.5 \times L/10$ have high fluctuations. The same responses in results of sd size are observed in nodal integration.

q is not effective on Gauss integration results of bending stress in Figure 26 for the simply supported beam (case II). However, a q value of 0.98 gives different stress responses in nodal integration in Figure 27.

4.3. L-shaped beam

Displacement results of the L-shaped beam (case III) are taken from the center of the beam in the x-direction. Bending stress results are taken from the middle of the upper surface of the beam. The RPIM with nodal and Gauss integration results is compared with FEM (ANSYS) solutions in Figures 28 and 29. The 1st order nodal integration includes fluctuations and cannot satisfy accuracy, but further orders of nodal integration and Gauss integration results with sampling points of 2×2, 3×3, and 4×4 have similar results as FEM (ANSYS).

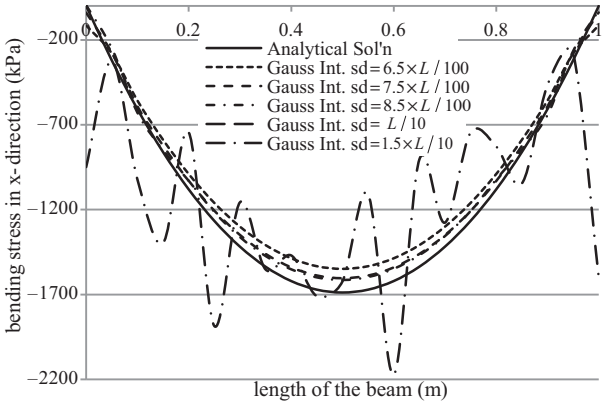

Figure 24. Comparison of effect of sd on bending stress results of distributed loaded simply supported beam (case II) for 4×4 Gauss int.

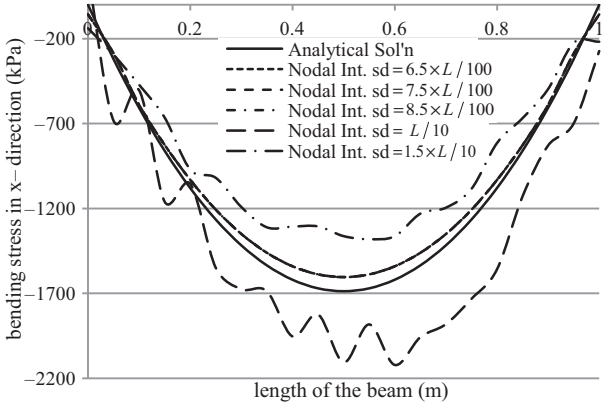

Figure 25. Comparison of effect of sd on bending stress results of distributed loaded simply supported beam (case II) for nodal int. (2 terms).

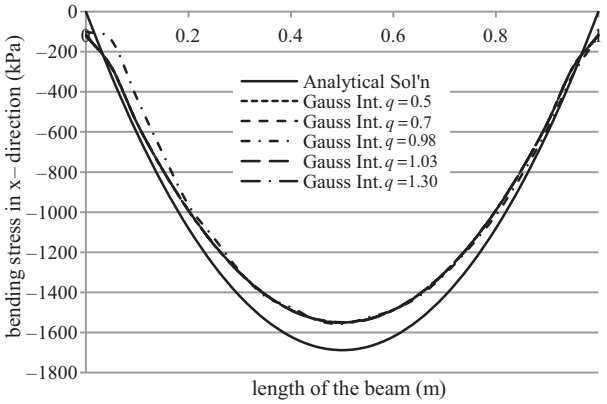

Figure 26. Comparison of effect of q on bending stress results of distributed loaded simply supported beam (case II) for 4×4 Gauss int.

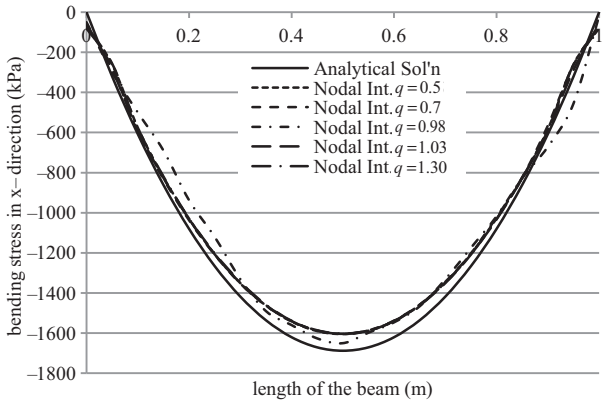

Figure 27. Comparison of effect of q on bending stress results of distributed loaded simply supported beam (case II) for nodal int. (2 terms).

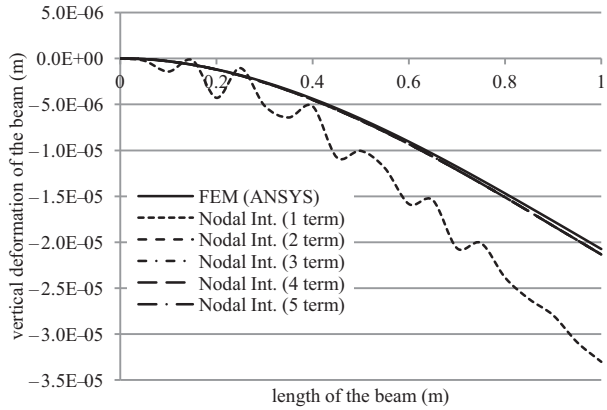

Figure 28. Comparison of vertical deformation results of L-shaped beam (case III) for FEM and nodal int. techniques.

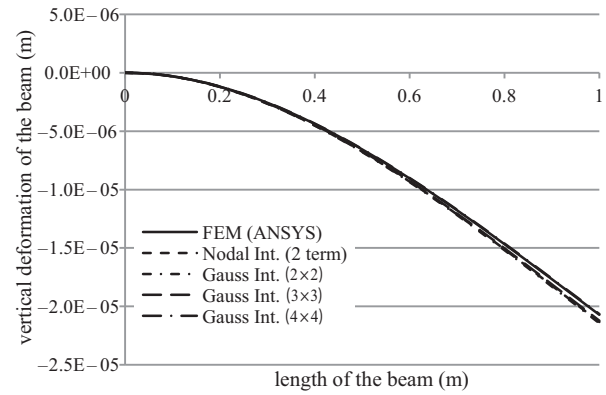

Figure 29. Comparison of vertical deformation results of L-shaped beam (case III) for FEM, Gauss, and nodal int. (2 terms) techniques.

Bending stress results for the L-shaped beam (case III) are given in Figures 30 and 31. Nodal integration with 1 term cannot satisfy accuracy and includes high fluctuations. The 2nd and further terms of nodal integration and Gauss integration results give suitable results with respect to the FEM (ANSYS), but a little difference occurs in the results.

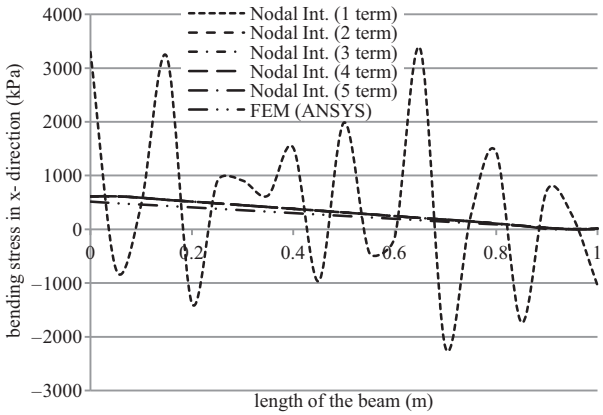

Figure 30. Comparison of bending stress results of L-shaped beam (case III) for FEM and nodal int. techniques.

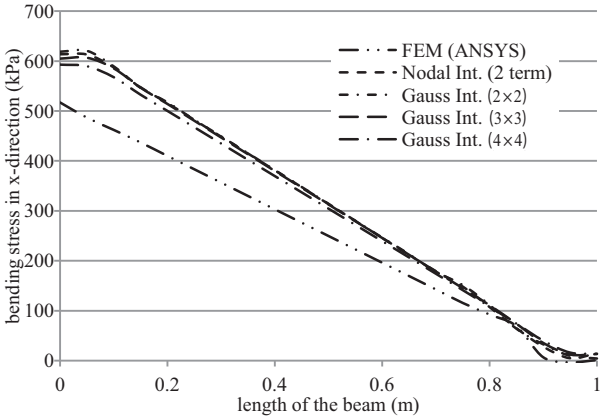

Figure 31. Comparison of bending stress results of L-shaped beam (case III) for FEM, Gauss, and nodal int. (2 terms) techniques.

Effects of α_c on deformation results of the L-shaped beam (case III) are given in Figures 32 and 33. It is shown that there is no α_c effect in Gauss integration results. α_c values of 1.00, 3.00, 5.00, and 9.00 have the same deformation results, but the α_c value of 7.00 has less accuracy in results of nodal integration.

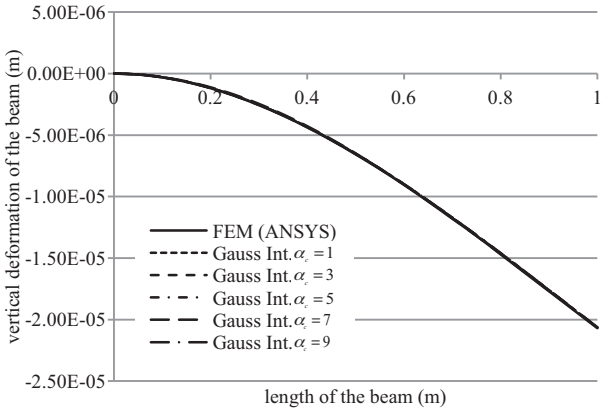

Figure 32. Comparison of effect of α_c on vertical deformation results of L-shaped beam (case III) for 4×4 Gauss int.

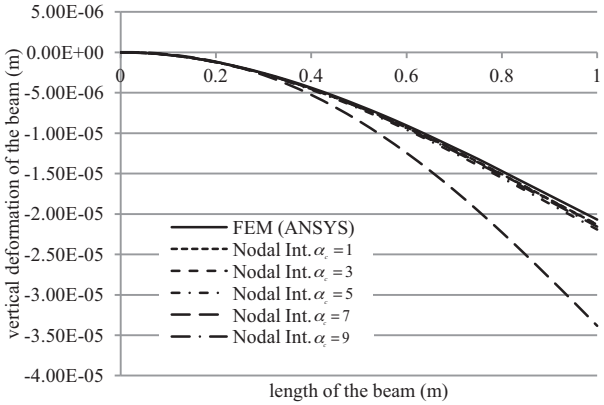

Figure 33. Comparison of effect of α_c on vertical deformation results of L-shaped beam (case III) for nodal int. (2 terms).

Effects of sd on deformation of the L-shaped beam (case III) are given in Figures 34 and 35. sd values of $6.5 \times L/100$, $7.5 \times L/100$, and $8.5 \times L/100$ in Gauss and nodal integration have the same results as the FEM (ANSYS) results. However, accuracy of the solution decreases when the sd value is increased to $L/10$ and $1.5 \times L/10$.

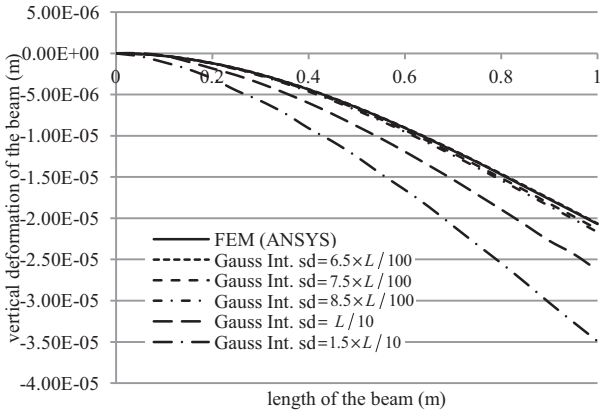

Figure 34. Comparison of effect of sd on vertical deformation results of L-shaped beam (case III) for 4×4 Gauss int.

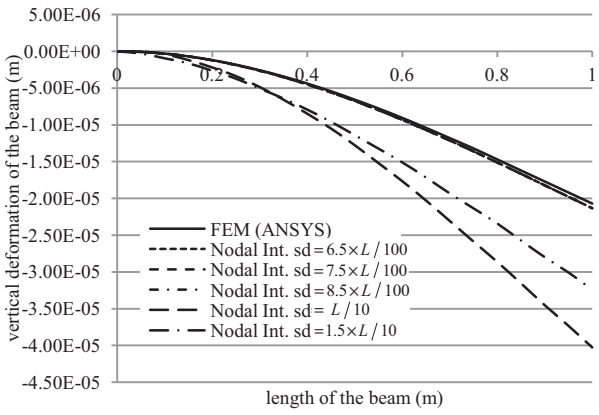

Figure 35. Comparison of effect of sd on vertical deformation results of L-shaped beam (case III) for nodal int. (2 terms).

In Figures 36 and 37, the effects of q for nodal and Gauss integration results are given for deformation results of the L-shaped beam (case III). There is no effect of q on results of Gauss integration. The q value of 0.98 has a difference in deformation results in nodal integration. Other deformation results of q values have same results.

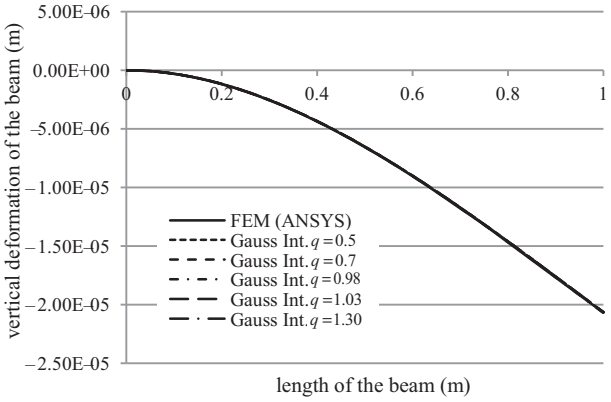

Figure 36. Comparison of effect of q on vertical deformation results of L-shaped beam (case III) for 4×4 Gauss int.

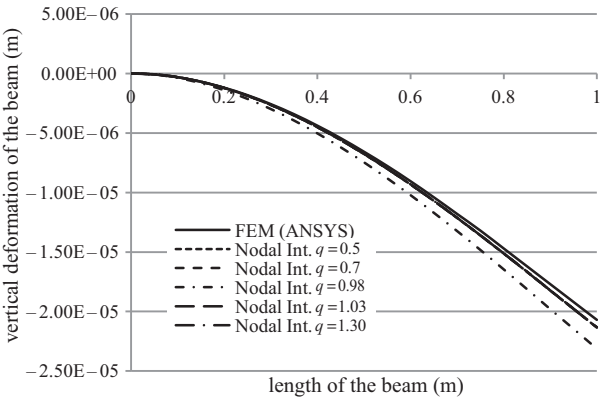

Figure 37. Comparison of effect of q on vertical deformation results of L-shaped beam (case III) for nodal int. (2 terms).

Bending stress results of the L-shaped beam (case III) are given in Figures 38 and 39 for various α_c values. It is detected that changes in α_c has no positive effects on either Gauss or nodal integrations. When an α_c value of 7.00 is used, high fluctuations in the results occur and accuracy is lost in nodal integration.

Effects of support domain sizes are given for the L-shaped beam (case III) in Figures 40 and 41. Results of sd values of $6.5 \times L/100$, $7.5 \times L/100$, and $8.5 \times L/100$ are similar and give sufficient accuracy in both Gauss and nodal integrations. However, sd values of $L/10$ and $1.5 \times L/10$ affect it negatively and cause high fluctuations in the results.

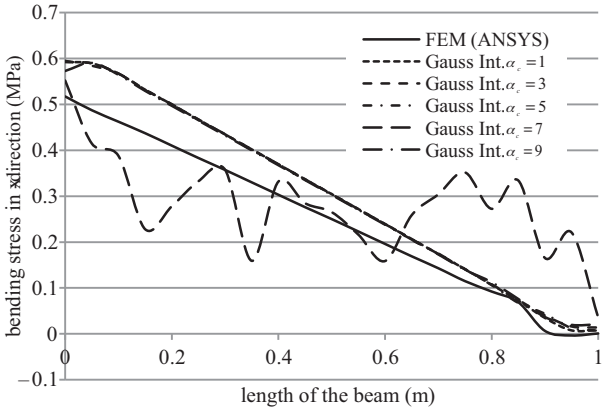

Figure 38. Comparison of effect of α_c on bending stress results of L-shaped beam (case III) for 4×4 Gauss int.

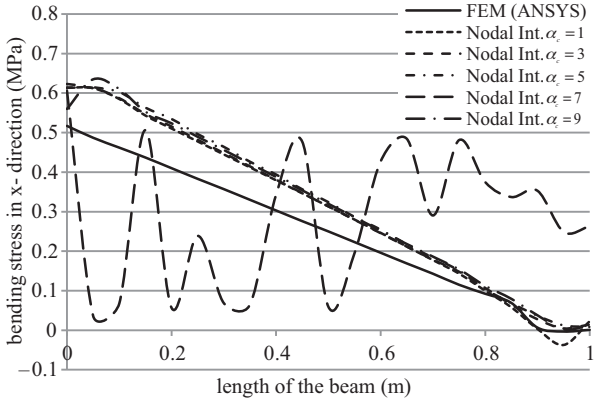

Figure 39. Comparison of effect of α_c on bending stress results of L-shaped beam (case III) for nodal int. (2 terms).

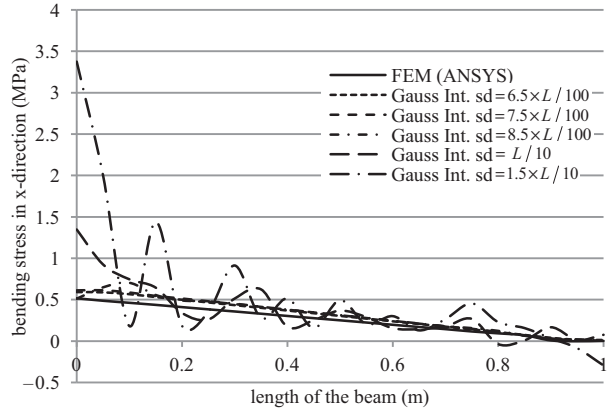

Figure 40. Comparison of effect of sd on bending stress results of L-shaped beam (case III) for 4×4 Gauss int.

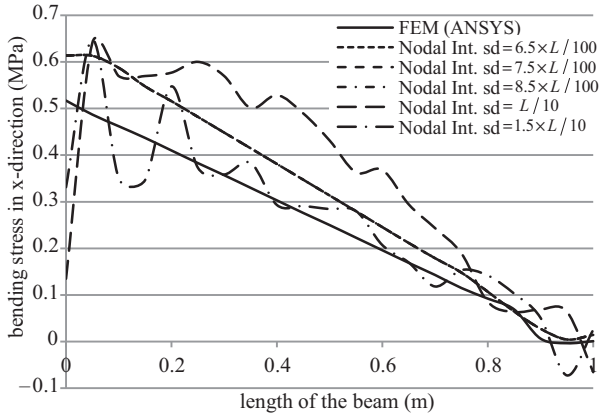

Figure 41. Comparison of effect of sd on bending stress results of L-shaped beam (case III) for nodal int. (2 terms).

Effects of various q values are given in Figures 42 and 43 for bending stress of the L-shaped beam. Without a q value of 0.98, all other q values have similar results in both nodal and Gauss integration.

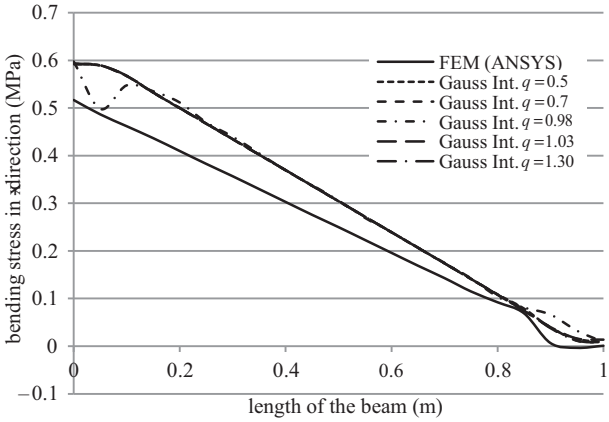

Figure 42. Comparison of effect of q on bending stress results of L-shaped beam (case III) for 4×4 Gauss int.

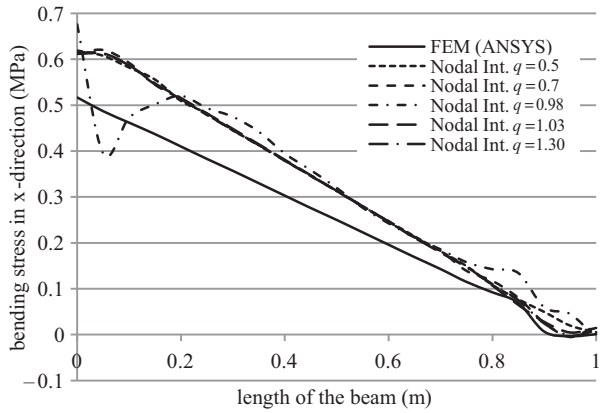

Figure 43. Comparison of effect of q on bending stress results of L-shaped beam (case III) for nodal int. (2 terms).

Solution times of the RPIM with nodal and Gauss integration techniques are approximately given in Table 5 for the simply supported beam. It is seen that usage of only the first term in nodal integration has the best solution time. When the used terms in nodal integration increase, solution time in nodal integration increases. The increment rate of solution time in nodal integration is greater than in Gauss integration.

Table 5. Comparison of solution times of RPIM with nodal and Gauss integration techniques for simply supported beam model of 189 nodes.

RPIM with nodal integration		Solution time (s)	Solution time (s)	RPIM with Gauss Gauss integration	
189 nodes	1 term	1.669	1.794	$2 \times 2 \times 2$	189 nodes
	2 terms	4.337	3.635	$3 \times 3 \times 3$	
	3 terms	11.107	6.084	$4 \times 4 \times 4$	
	4 terms	30.466			
	5 terms	55.724			

5. Conclusion

Two different integration techniques (nodal and Gauss) are used for RPIM solutions and their effects on 3D elastostatic solutions are investigated. Taylor series expansion is used in nodal integration and investigated up to the 5th order, and 2×2, 3×3, and 4×4 numbers of sampling points are used in Gauss integration. In addition, effects of shape parameters and support domain sizes are also investigated. Results are summarized as follows:

- Usage of a single term of the Taylor series expansion in nodal integration cannot satisfy accuracy with respect to analytical solutions.
- Nodal integrations with second and higher order of terms give sufficient results and they have better performance than the FEM (ANSYS) in some cases.
- The 2nd, 3rd, 4th, and 5th order terms of nodal integration give nearly the same results.
- Gauss integration in the RPIM also gives good results in all numbers of sampling points.
- For solutions of computational fluid dynamics (CFD) problems, it is mentioned in the literature [35] that 1st order Taylor series expansion is not enough. The usage of second order terms is recommended for most CFD applications. The same situation is also valid and detected in this study for nodal integration.
- Shape parameter α_c is not effective on Gauss integration results in cases II and III. However, when α_c is equal to 7.00 in nodal integration results, the accuracy of the solution vanishes. α_c values of 7.00 and 9.00 cause failure in construction of shape function in case I.
- Support domain sizes of $6.5 \times L/100$, $7.5 \times L/100$, and $8.5 \times L/100$ of both nodal and Gauss integration give good agreements with analytical and FEM solutions in cases II and III. However, increasing support domain size to $L/10$ and $1.5 \times L/10$ causes a decrease in accuracy. sd values of $8.5 \times L/100$, $L/10$, and $1.5 \times L/10$ in Gauss integration cannot support construction of shape functions in case I.
- Shape parameter q is not effective in Gauss integration. Similar results are also obtained in nodal integration. However, when q is equal to 0.98, accuracy decreases in nodal integration solutions. q values of 0.5 and 0.98 cause failures in Gauss integration in case I. When q is used as a different value from 1.03, the results include high fluctuations.

References

[1] Gingold RA, Monaghan JJ. Smoothed particle hydrodynamics: theory and application to non-spherical stars. Mon Not R Astron Soc 1977; 181: 375-389.

[2] Lucy LB. A numerical approach to the testing of the fission hypothesis. Astron J 1977; 82: 1013-1024.

[3] Libersky LD, Petschek AG. Smooth particle hydrodynamics with strength of materials. Lect Notes Phys 1991; 395: 248-257.

[4] Libersky LD, Petschek AG, Carney TC, Hipp JR, Allahdadi FA. High strain Lagrangian hydrodynamics: a three-dimensional SPH code for dynamic material response. J Comput Phys 1993; 109: 67-75.

[5] Nayroles B, Touzot G, Villon P. Generalizing the finite element method: diffuse approximation and diffuse elements. Comput Mech 1992; 10: 307-318.

[6] Belytschko T, Lu YY, Gu L. Element-free Galerkin methods. Int J Numer Methods Eng 1994; 37: 229-256.

[7] Liu WK, Chen Y, Chang CT, Belytschko T. Advances in multiple scale kernel particle methods. Comput Mech 1996; 18: 73-111.

[8] Atluri SN, Zhu T. A new meshless local Petrov-Galerkin (MLPG) approach in computational mechanics. Comput Mech 1998; 22: 117-127.

[9] Liu GR, Gu YT. A point interpolation method for two-dimensional solids. Int J Numer Meth Eng 2001; 50: 937-951.

[10] Liu GR, Gu YT. A local radial point interpolation method (LR-PIM) for free vibration analyses of 2-D solids. J Sound Vib 2001b; 246: 29-46.

[11] Chen W, Tanaka M. Meshless, integration-free, and boundary-only RBF technique. Comput Math Appl 2002; 43: 379-391.

[12] Liu GR, Gu YT. Boundary meshfree methods based on the boundary point interpolation methods. Eng Anal Bound Elem 2004; 28: 475-487.

[13] Liu GR, Zhang GY, Dai KY. A linearly conforming point interpolation method (LC-PIM) for 2D solid mechanics problems. Int J Comput Meth 2005; 2: 645-665.

[14] Liu GR, Zhang GY, Wang YY, Zhong ZH, Li GY, Han X. A nodal integration technique for meshfree radial point interpolation method (NI-RPIM). Int J Solid Struct 2007; 44: 3840-3860.

[15] Wu SC, Liu GR, Zhang HO, Xu X, Li ZR. A node-based smoothed point interpolation method (NS-PIM) for three-dimensional heat transfer problems. Int J Thermal Sci 2009; 48: 1367-1376.

[16] Cui XY, Liu GR, Li GY. A cell-based smoothed radial point interpolation method (CS-RPIM) for static and free vibration of solids. Eng Anal Bound Elem 2010; 34: 144-157.

[17] Wu SC, Liu GR, Cui XY, Nguyen TT, Zhang GY. An edge-based smoothed point interpolation method (ES-PIM) for heat transfer analysis of rapid manufacturing system. Int J Heat Mass Tran 2010; 53: 1938-1950.

[18] Dinis LMJS, Jorgea RMN, Belinha J. Analysis of 3D solids using the natural neighbour radial point interpolation method. Comput Method Appl M 2007; 196: 2009-2028.

[19] Dinis LMJS, Jorgea RMN, Belinha J. Analysis of plates and laminates using the natural neighbour radial point interpolation method. Eng Anal Bound Elem 2008; 32: 267-279.

[20] Wang JG, Liu GR. On the optimal shape parameters of radial basis functions used for 2-D meshless methods. Comput Method Appl M 2002; 191: 2611-2630.

[21] Kanber B, Bozkurt OY, Erklig A. Investigation of RPIM shape parameter effects on the solution accuracy of 2D elastoplastic problems. Int J Comput Meth Eng Sci Mech 2013; 14: 354-366.

[22] Bozkurt OY, Kanber B, Asik MZ. Assessment of RPIM shape parameters for solution accuracy of 2D geometrically nonlinear problems. Int J Comput Meth 2013; 10: 1-26.

[23] Aliabadi MH, Hall WS, Phemister TG. Taylor expansion for singular kernels in the boundary element method. Int J Numer Meth Eng 1985; 21: 2221-2236.

[24] Arad M, Segev R, Ben-Dor G. Accuracy increase of finite difference calculations on arbitrary meshes by means of differentiation of the partial differential equations and their boundary conditions. Comput Struct 1997; 64: 541-552.

[25] Iwashige K, Yokota N. Numerical simulation of turbulent shear flow using higher order Taylor series expansion method. J Nucl Sci Technol 1995; 32: 30-41.

[26] Fosso PA, Deniau H, Sicot F, Sagaut P. Curvilinear finite-volume schemes using high-order compact interpolation. J Comput Phys 2010; 229: 5090-5122.

[27] Abbas K, Heidergott B, Aissani D. A Taylor series approach to the numerical analysis of the m/d/1/n queue. Procedia Computer Science 2012; 1: 1553-1560.

[28] Tari H. On the parametric large deflection study of Euler-Bernoulli cantilever beams subjected to combined tip point loading. Int J Nonlin Mech 2013; 49: 90-99.

[29] Yavuz MM, Kanber B. Effect of higher order Taylor series expansion terms of the NI-RPIM on the solution accuracy of 2D elastic problems. Pamukkale University Journal of Engineering Sciences 2015; 21: 1-10.

[30] Liu GR, Gu YT. An Introduction to Meshfree Methods and Their Programming. Berlin, Germany: Springer, 2005.

[31] Liu GR. Meshfree Methods: Moving Beyond the Finite Element Method. 2nd ed. Boca Raton, FL, USA: CRC Press, 2009.

[32] Yavuz MM, Kanber B. On the usage of tetrahedral background cells in nodal integration of RPIM for 3D elasto-static problems. Int J Comput Meth 2015; 12: 1-30.

[33] Beer FP, Johnston ER Jr, Dewolf JT, Mazurek DF. Mechanics of Materials. 5th ed. Singapore: McGraw-Hill Press, 2009.

[34] Timoshenko S, Goodier JN. Theory of Elasticity. Toronto, Canada: McGraw-Hill Book Company, 1951.

[35] Anderson JD. Computational Fluid Dynamics: The Basics with Applications. New York, NY, USA: McGraw-Hill Press, 1995.